Science of the Total Environment 799 (2021) 149346

Contents lists available at ScienceDirect

Science of the Total Environment

journal homepage: www.elsevier.com/locate/scitotenv

Characterization of the main land processes occurring in Europe (2000-2018) through a MODIS NDVI seasonal parameter-based procedure

J.M. Ramírez-Cuesta [a,*], M. Minacapilli [b], A. Motisi [b], S. Consoli [c], D.S. Intrigliolo [d], D. Vanella [c]

[a] Dpto. Riego, Centro de Edafología y Biología Aplicada del Segura (CEBAS-CSIC), P.O. Box 164, 30100 Murcia, Spain
[b] Dipartimento di Scienze Agrarie, Alimentari e Forestali (SAAF), Università degli Studi di Palermo, V.le delle Scienze Ed. 4, 90128 Palermo, Italy
[c] Dipartimento di Agricoltura, Alimentazione e Ambiente (Di3A), Università degli Studi di Catania, Via S. Sofia, 100, 95123 Catania, Italy
[d] Department of Ecology, Desertification Research Centre (CIDE-CSIC-UV-GV), 46113 Moncada, Valencia, Spain

HIGHLIGHTS

- MODIS NDVI time series for characterizing land processes at continental scale
- Seasonal parameters for retrieving temporal evolution of land uses
- Maximum and Large Integrated parameters characterize most of evaluated processes
- Limitation to detect land processes involving land uses with similar NDVI trends
- Methodology useful for addressing the United Nations sustainable development goals

GRAPHICAL ABSTRACT

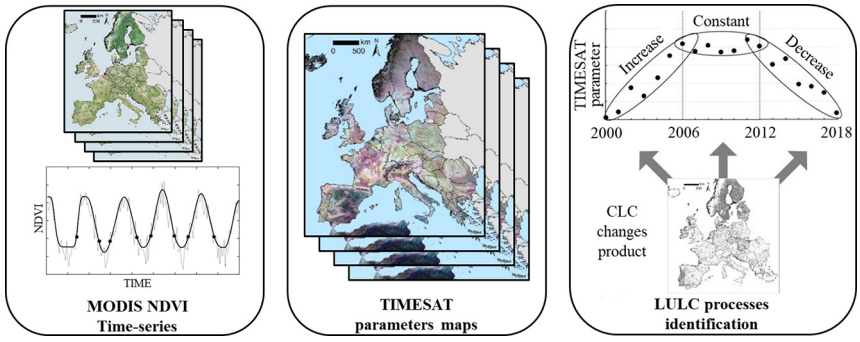

ARTICLE INFO

Article history:
Received 12 March 2021
Received in revised form 6 July 2021
Accepted 26 July 2021
Available online 31 July 2021

Editor: Martin Drews

Keywords:
TIMESAT
Normalized difference vegetation index
CORINE
Land use
Land cover

ABSTRACT

The identification and recognition of the land processes are of vital importance for a proper management of the ecosystem functions and services. However, on-ground land uses/land covers (LULC) characterization is a time-consuming task, often limited to small land areas, which can be solved using remote sensing technologies. The objective of this work is to investigate how the different MODIS NDVI seasonal parameters responded to the main land processes observed in Europe in the 2000-2018 period; characterizing their temporal trend; and evaluating which one reflected better each specific land process. NDVI time-series were evaluated using TIMESAT software, which extracted eight seasonality parameters: amplitude, base value, length of season, maximum value, left and right derivative values and small and large integrated values. These parameters were correlated with the LULC changes derived from COoRdination of INformation on the Environment Land Cover (CLC) for assessing which parameter better characterized each land process. The temporal evolution of the maximum seasonal NDVI was the parameter that better characterized the occurrence of most of the land processes evaluated (afforestation, agriculturalization, degradation, land abandonment, land restoration, urbanization; R^2 from 0.67-0.97). Large integrated value also presented significant relationships but they were restricted to two of the three evaluated periods. On the contrary, land processes involving CLC categories with similar NDVI patterns were not well captured with the proposed methodology. These results evidenced that this methodology could be combined with other classification methods for improving LULC identification accuracy or for identifying LULC processes in locations where no LULC maps are available. Such information can be used by policy-makers to draw

* Corresponding author.
E-mail address: ramirezcuesta.jm@gmail.com (J.M. Ramírez-Cuesta).

https://doi.org/10.1016/j.scitotenv.2021.149346

LULC management actions associated with sustainable development goals. This is especially relevant for areas where food security is at stake and where terrestrial ecosystems are threatened by severe biodiversity loss.

1. Introduction

Earth surface furnishes the basis for many ecosystem functions and services essential for human society. In the last decades, the land uses/land covers (LULC) have experienced significant changes mainly due to climate change (CC) and anthropogenic activities, modifying both LULC extent and distribution at global scale (Grimm et al., 2008; Seto and Satterthwaite, 2010; Ramírez-Cuesta et al., 2016). Generally, LULC changes, especially those derived from CC, lead to an increase of ecosystems vulnerability, compromising its capacity to maintain food production and natural resources, control climate and air quality, and lessen infectious diseases (Sala et al., 2000; Foley et al., 2005). The magnitude of these risks depends on several factors, including the warming and population patterns, the exploitation of natural resources, the technological advances, and the environmental management strategies (IPCC, 2019).

Important actions for minimizing negative impacts on the different societal sectors due to LULC changes mainly consist of the design of multi-level and integrated policies for the sustainable planning and management (Di Gregorio et al., 2019). At European level, a concrete example of these actions is CORINE (COoRdination of INformation on the Environment) Land Cover (CLC) programme conducted by the European Environment Agency, which provides an inventory on LULC every 6 years since the 90s (2000, 2006, 2012 and 2018) (https://land.copernicus.eu/pan-european/corine-land-cover). This programme takes advantage of Earth observation satellite data for periodically covering wide extensions of terrain in a single image, allowing identifying past LULC trends and predicting future patterns.

At present, there exist several satellite sensors (e.g. from MODIS to Sentinel-2A/B) for LULC mapping by using surface reflectance values or indices generated from remote sensing imaging bands (e.g. Normalized Difference Vegetation Index, NDVI; Soil Adjusted Vegetation Index, SAVI; and Enhanced Vegetation Index, EVI). A number of approaches have been developed for LULC classification, including those based on spectral or spectral-spatial features (Shao et al., 2016; Ma et al., 2017), on deep learning techniques (Zhao and Du, 2016; Paoletti et al., 2018; Zhang et al., 2018) and on multi-source data fusion techniques (Chen et al., 2017; Zhang and Xu, 2018). Most of the approaches converge in highlighting the critical role of the temporal profile for LULC identification, which provides a more accurate classification than when using single images. In this sense, new ways of performing LULC classifications have been opened up also for land processes detection thanks to the availability of long time-series satellite images. This is the case of Landsat Mission, publicly available since 1972; and the synergy of Terra and Aqua satellites, with Moderate-Resolution Imaging Spectroradiometer (MODIS) on board, which in 2019 celebrated its 20th anniversary (1999-2019). These satellites allow obtaining high-frequency LULC maps and, by its comparison, identifying, characterizing and monitoring the main land processes acting in the territory.

Authors have proposed several approaches for identifying and monitoring LULC changes with different level of complexity and accuracy (Mallinis et al., 2014; Quintero-Gallego et al., 2018; Luo et al., 2020). In general terms, these approaches can be divided into post-classification and time-series change detection methods (Yan et al., 2019). The post-classification change detection methods consist on comparing two images taken at different moment and classifying the changes based on the indicators discrepancies between the two dates (Pontius et al., 2004; Ramírez-Cuesta et al., 2016; Luo et al., 2020). The second group, the time series change detection methods, considers longer temporal periods, requiring a higher number of satellites images over a reference time period for LULC change detection. They include the use of thresholds (Xie and Weng, 2016; Venkatappa et al., 2019), the slope evaluation of a fitted curve (Jönsson and Eklundh, 2004; Bradley et al., 2007) and the comparison and segmentation of trajectories with training signatures specific for different LULC changes (Kennedy et al., 2007; Maciel et al., 2019). According to Gholamnia et al. (2019), the time series change detection methods can be further distinguished in abrupt/gradual changes methods (i.e. based on spectral frequency and statistical approaches; e.g. BFAST, Verbesselt et al., 2010; COLD, Zhu et al., 2019) and seasonal parameters based approaches (e.g.; HANTS, Zhou et al., 2015; PhenoSat, Rodrigues et al., 2016; TIMESAT, Jönsson and Eklundh, 2004).

Commonly, the seasonal parameter based approaches evaluate directly the VI values trend performing a previous smoothing of VI pixel curves (Shao et al., 2016; Novillo et al., 2019) Nevertheless, in literature, less attention has been paid to the use of seasonal parameters for mapping spatial or temporal changes in the vegetation cover resulting from LULC changes (e.g., beginning, end and amplitude of the growing season) (Jia et al., 2014). Despite the advances reached in the field of the methodologies proposed for detecting and quantifying spatiotemporal patterns of land cover changes, it is still difficult to capture the significance of land cover changes over time (Waylen et al., 2014). The main advantage of the use of the seasonal parameters is that it helps to overcome any inconsistency caused by punctual malfunctioning of remote sensing imagery. Today, only MODIS sensor offers two decades of NDVI time series with 8/16 days of temporal resolution. With this unique feature, MODIS time series products are suitable to better understand the environmental dynamics that drive the LULC changes and not only to map "what it is today" compared to the past.

The present study goes beyond an identification of LULC and its temporal changes, attempting to characterize the main land processes in terms of the temporal evolution of eight different seasonal parameters. Therefore, the main objectives of this work are (i) to investigate how the different MODIS NDVI seasonal parameters responded to the main land processes observed in Europe in the 2000-2018 period; (ii) to characterize their temporal trend; and (iii) to evaluate which one reflected better each specific land process.

2. Materials and methods

The methodology adopted in the present study for identifying and characterizing the main land processes in Europe is summarized in Fig. 1. A detailed description of the data inputs and the seasonal parameter-based procedure are reported in the next sub sections.

2.1. Remote sensing imagery

NDVI time-series for entire Europe covering the 2000-2018 period (Fig. 1A) were obtained from MODIS vegetation indices product (MOD13A2; Didan, 2015; https://lpdaac.usgs.gov/products/mod13a2v006/). This product provides the most representative VI value at 1 km spatial resolution, from all the acquisitions each 16-days period, in function of the cloud mask (Ackerman et al., 1996), atmospheric correction (Vermote et al., 1997), view zenith angle, solar zenith angle, relative azimuth angle, geo-registration (Wolfe et al., 1998), and surface BRDF normalization. In this study, only Terra satellite was considered for creating the VI time-series, since Aqua does not cover the complete reference period, avoiding also possible inconsistencies

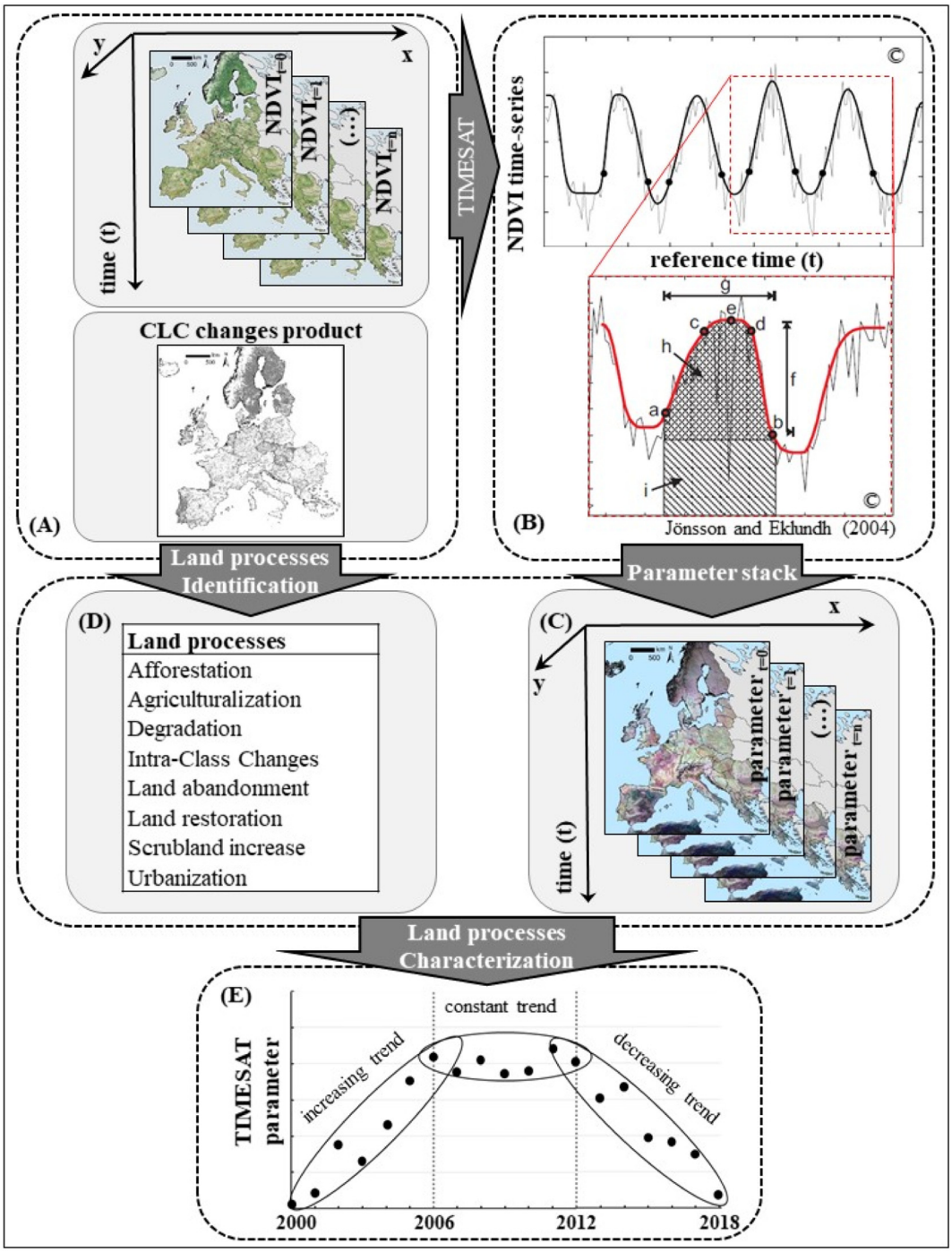

Fig. 1. Flow chart of the proposed methodology to evaluate the use of seasonal parameters for characterizing land processes. For a description of the symbols included in panel B the reader is referred to Sub-section "2.2 Time-series assessment".

between the spectral radiances detected by both MODIS satellites (Xiong et al., 2007; Minnis et al., 2008a, 2008b; Wenny et al., 2010).

MODIS VI products were downloaded through the National Aeronautics and Space Administration (NASA) Earthdata service (https://search.earthdata.nasa.gov/) in Hierarchical Data Format - Earth Observing System (HDF-EOS) format. All steps of the MODIS VI pre-processing workflow (i.e. downloading, compositing time series and extracting raw binary layers; Fig. 1A) were automated through scripts developed in a Linux environment. In particular, all operations were performed on a "tile by tile"/"pixel-by-pixel" basis with no attempt to perform mosaicking/reprojections operations, maintaining the native Integerized Sinusoidal MODIS projection throughout the whole processing. For this purpose, relevant layers were extracted as raw binaries through a simple command-line tool (called "hdf2rb") in the MODIS Reprojection Tool software suite (USGS-EROS Center, 2011). The raw binary layers extracted were directly usable by the TIMESAT software (see Section 2.2), after associating a suitable header file conforming to the IDRISI raster format, that contained the required geometry and georeferencing metadata (Eklundh and Jönsson, 2017).

Overall, a total of 6624 NDVI images were utilized in this study, spread in 23 images per year and tile, covering 16 tiles for Europe (i.e., tiles corresponding with "h" values between 17 and 20; and "v" values from 02 to 05).

2.2. Time-series assessment

A proper analysis of VI time-series derived from remote sensing provides useful information on seasonal parameters changes. For this purpose, TIMESAT 3.3 software (Eklundh and Jönsson, 2017; Jönsson and Eklundh, 2002, 2004; http://web.nateko.lu.se/timesat/timesat.asp) was adopted using MODIS VI time-series as input. This software allows processing VI time-series by smoothing each observed temporal trend to a fitted function (Fig. 1B). Specifically, TIMESAT implements three smoothing methods based on least-squares fits: Savitzky-Golay, asymmetric Gaussians and double logistic functions. From the fitted functions, TIMESAT extracts seasonality parameters that make possible to depict spatial or temporal VI changes due to LULC changes (Fig. 1B). The seasonality parameters outputted from TIMESAT include: (a) amplitude (Amp), (b) base value (Base), (c) length of season (Length), (d) maximum value (Max), (e) left and (f) right derivative values (Lder and Rder, respectively) and (g) small and (h) large integrated values (Sinteg and Linteg, respectively).

Table 1 shows the inputs referring to the Common settings used for processing the imagery pixel-by-pixel. More specifically, the Image files option was selected as the image mode as the data input was stored in image files (NDVI raster). No Seasonal Trend decomposition by LOESS (STL) trend fitting was applied since it has been noted that seasonal components extracted using STL have generally less accuracy than those obtained from other smoothing approaches (Eklundh and Jönsson, 2017). No quality data was provided due to the undisputed quality of MODIS input data already checked in MOD13A2 product (Huete et al., 1999). As Image file list input, a text file was elaborated according to the protocol proposed by Eklundh and Jönsson (2017), including an initial row reporting the number of VI images used, followed by the path and name of each VI image in separate lines. Image file type was fixed as 16-bit signed integer in little-endian byte order, coinciding with the data type of MOD13A2 product (Didan et al., 2015). Rows and columns number were assigned to 1200 as MOD13A2 tile size and the entire image was selected for processing (rows and columns to process from 1 to 1200). The Range of values varied between −2000 and 10,000 as specified in the MOD13A2 product specifications (Didan et al., 2015). The Number of years and the Number of data point per year were defined by the imagery dataset collected in this study, i.e., 18 and 23, respectively. Neither cutoff for low amplitude nor spike removal was applied, fixing consequently both parameters to 0. In the output data, it was selected to print the seasonality data and the fitted function. Additionally, no land cover data file was used whereas STL stiffness was fixed as its default value equal to 3. No debug data was printed.

Table 1
Common settings inputs used in TIMESAT for this study.

Common settings input	Value
Image mode	Image files
Trend	No trend
Quality	No quality data
Image file list	Text file
Image file type	16-bit signed integer
Byte order	Little endian
No of rows	1200
No of columns	1200
Rows to process	From 1 to 1200
Columns to process	From 1 to 1200
Range of values	From −2000 to 10,000
No of years	18
No of data point per year	23
Amplitude cutoff	0
Spike method	0
Output data	Seasonality, Fitted data and no original data
Use land data	0
STL stiffness	3
Debug Flag	0

Class specific settings used in the present study are listed in Table 2. Since no land cover data has been used in TIMESAT (see Table 1), code input was fixed to 1. The seasonality parameter equal to 1 was selected as recommended for fitting one season per year (Didan et al., 2015). No adaptation to the envelope was applied, specifying 1 for the number of envelope iterations, being therefore pointless the incorporation of a value for the adaptation strength input. The fitted function was not forced to a minimum value, fixing a value of 0 for this input. The double logistic approach was selected as fitting function as recommended by Didan et al. (2015) when handling rough temporal patterns as those observed in the NDVI time-series used in this study. The seasonal amplitude was selected as the start of season method, fixing 20% of the amplitude as the value for defining the start and the end of the season.

Once the seasonal parameters for each pixel were calculated (Fig. 1B), they were transformed into 8 multiband images (one image for each Timesat seasonal parameter) with 18 bands (each one corresponding with a season) (Fig. 1C). This operation was performed through a script developed in a Linux environment.

2.3. CORINE land cover

CLC inventories for the years 2000, 2006, 2012 and 2018 were used as the reference for the identification of the main LULC transitions occurring in the European territory. CLC categories are arranged in 3 levels in a nested hierarchy as function of the details level. Level-1 is the most generalist or aggregated classification, distinguishing 5 categories: (1) artificial surfaces; (2) agricultural areas; (3) forest and semi-natural areas; (4) wetlands; and (5) water bodies. Level-2 and Level-3 provide more detailed classifications, with 15 and 44 LULC categories, respectively. Therefore, each LULC category is defined by a three-numbers code; the first referring to the Level-1 classification and the second and third to the Level-2 and Level-3, respectively. The complete legend of CLC level classifications including their structure and class descriptions can be found in Kosztra et al. (2017).

CLC is generally generated by visual interpretation of high-resolution satellite imagery (including e.g., Landsat-7 ETM+, Landsat 8 OLI/TIRS, SPOT-4/5, IRS P6 LISS III, RapidEye and Sentinel-2), although semi-automatic approaches combining in-situ data, satellite image and Geographic Information Systems (GIS) are becoming more frequently used. For the identification of the LULC transitions, CLC-Changes vector layers for the 2000-2006, 2006-2012 and 2012-2018 periods were utilized (Fig. 1A; https://land.copernicus.eu/pan-european/corine-land-cover). These layers compare CLC of successive surveys, detecting areas where LULC changed, with a minimum mapping unit of 5 ha.

2.4. Land processes identification

The main land processes acting in the European territory were selected on the basis of literature review (Gómez-Mendoza et al., 2006; Mendoza et al., 2011; Lasanta and Vicente-Serrano, 2012; Teixeira et al., 2014; Ramírez-Cuesta et al., 2016; Levers et al., 2018; Yin et al., 2018a, 2018b; Lu et al., 2019; Nguyen et al., 2020; Zhu et al., 2021). Thus, according to these authors, the main land processes considered in this study were afforestation (Aff), agriculturalization (Agr),

Table 2
Class specific settings inputs used in TIMESAT for this study.

Class specific settings input	Value
Code	1
Seasonal par. (0-1)	1
No. envelope iterations	1
Force minimum value	0
Fitting method	Double logistic
Start of season method	Seasonal amplitude
Season start value	0.2
Season end value	0.2

agricultural change (AgrCh), artificial use change (ArtCh), degradation (Deg), land abandonment (LAbn), land restoration (LRst), scrubland increase (Scr), urbanization (Urb) and wetlands and water bodies change (WBCh). Afforestation refers to the expansion of forest cover at the expense of other LULC. Agriculturalization implies the transformation of non-agricultural LULC categories in agricultural ones. Agricultural, artificial and wetlands and water bodies changes refers to changes in LULC but limited between agricultural, artificial and wetlands and water bodies categories, respectively. Urbanization refers to the growth of urban LULC categories in areas previously occupied by other LULC. Land abandonment is considered as the transformation of artificial surfaces and agricultural areas into forest or semi natural areas. Land restoration takes into account the gain of wetlands or water bodies areas at the expense of other LULC types. Degradation reflects a transition to a less dense natural vegetation LULC. Scrubland increase refers to the encroachment of scrub into previously natural areas with open spaces with little or no vegetation.

The land processes identification was performed starting from the LULC transitions obtained from CLC-Changes product (see Section "2.3 CORINE Land Cover") (Fig. 1D), associating later to each LULC transition the related process (Table 3), as indicated in Fig. 2.

In order to integrate MOD13A2 product and CLC-Changes data sources, after the assignation of the corresponding land processes occurring in each feature, the CLC-Changes vector shapefile was converted into a raster file, fixing the same spatial resolution (i.e. cell size of 1 km) and extension than MOD13A2 product. Such procedure was performed by following a majority approach, assuming that the land process occurring within a pixel correspond with the prevailing one (i.e. the land process covering the largest proportion of the pixel).

2.5. Statistical analysis

The performance of the seasonality parameters retrieved as described in Section "2.2. Time-series assessment" for identifying the main land processes occurred in Europe was evaluated by analysing their temporal evolution at each reference period (2000-2006, 2006-2012 and 2012-2018) (Fig. 1E). In this sense, ArcGIS (v10.2; Esri, Redlands, CA, USA) was used for extracting the land processes (from CLC-Changes dataset in raster format) and seasonal parameters values (from TIMESAT outputs) at pixel level. Then, the temporal trends of the different seasonal parameters were evaluated considering its average values for each land process and temporal period (i.e. 2000-2006, 2006-2012 and 2012-2018). These temporal patterns were adjusted to linear functions characterized by a slope term and a coefficient of determination, R^2.

The sign of the slope term reflects if a determined land process produces an increase (slope > 0) or a decrease (slope < 0) in the seasonality parameter assessed. The absolute slope value gives an idea of the phenomena magnitude for each seasonality parameter, being the land process more abrupt as the absolute slope value is greater. R^2 was used for assessing the goodness of fit, indicating the proportion of the relationship variation explained by the different seasonality parameters.

For validation purposes, the entire dataset was split into training and validation sets, containing the 60 and 40% of the data for each LULC, respectively. The significance of the relationships obtained from the training and validation sets (in terms of their slopes) was evaluated by performing one-way analysis of variance (ANOVA) with *post-hoc* Tukey HSD test for its comparison.

3. Results

3.1. Land processes quantification

From the CLC change maps of the three considered periods (2000-2006, 2006-2012 and 2012-2018), it can be derived that the most dynamic period corresponded with the 2006-2012, with near 88.000 km^2 experimenting some LULC change (1.7% of the total area; Table 3). The 2000-2006 and 2012-2018 periods identified LULC changes in approximately 66.000 and 67.500 km^2, respectively ($\approx$ 1.3% of the total area; Table 3). However, LULC changes were not homogeneous among all evaluated nations. There were countries with LULC changes of less than 0.5% of its total surfaces in all periods (e.g. Austria, Slovenia and Switzerland) whereas other countries reach LULC change rates higher than 3.5% of its total area in some of the periods (e.g. Estonia, Portugal and Sweden in 2006-2012 and 2012-2018) (Fig. 3). Regarding the land processing quantification, the predominant phenomena affecting the territory were degradation, afforestation, agricultural change, and urbanization representing the 45.9, 29.0, 8.8 and 7.2% of the total LULC changes, respectively (Table 3).

3.2. Seasonal parameters representativeness

After quantifying the LULC changes occurred in Europe during the period 2000-2018, the representativeness of the seasonality parameters to characterize these land processes was assessed for the 2000-2006

Table 3
Area (km^2) affected by each considered land process for the different temporal periods evaluated (2000-2006, 2006-2012 and 2012-2018).

Land process		Code	2000-2006 (km^2)	2006-2012 (km^2)	2012-2018 (km^2)
Afforestation	From 1XX	Aff_1	9. (0.0%)	22 (0.0%)	6 (0.0%)
	From 2XX	Aff_2	169 (0.3%)	95 (0.1%)	56 (0.1%)
	From 3XX	Aff_3	11,818 (17.9%)	35,168 (40.1%)	18,249 (27.0%)
	From 4XX/5XX	$Aff_{4,5}$	483 (0.7%)	261 (0.3%)	298 (0.4%)
Agriculturalization	From 1XX	Agr_1	256 (0.4%)	282 (0.3%)	347 (0.5%)
	From 3XX	Agr_3	1568 (2.4%)	680 (0.8%)	1045 (1.6%)
	From 4XX/5XX	$Agr_{4,5}$	234 (0.4%)	53 (0.1%)	184 (0.3%)
Degradation		Deg	33,864 (51.2%)	32,288 (36.8%)	33,538 (49.7%)
Intra-Class Changes	Agricultural	AgrCh	5283 (8.0%)	7840 (8.9%)	6407 (9.5%)
	Artificial use	ArtCh	1218 (1.8%)	1571 (1.8%)	1202 (1.8%)
	Wetlands and water bodies	WBCh	32 (0.1%)	31 (0.0%)	44 (0.1%)
Land abandonment	From 1XX	$LAbn_1$	257 (0.4%)	178 (0.2%)	193 (0.3%)
	From 2XX	$LAbn_2$	1721 (2.6%)	1742 (2.0%)	898 (1.3%)
Land restoration	From 1XX	$LRst_1$	99 (0.2%)	105 (0.1%)	89 (0.1%)
	From 2XX	$LRst_2$	377 (0.6%)	398 (0.5%)	233 (0.4%)
	From 3XX	$LRst_3$	495 (0.8%)	445 (0.5%)	304 (0.5%)
Scrubland increase		Scr	1526 (2.3%)	1176 (1.3%)	902 (1.3%)
Urbanization	From 2XX	Urb_2	5276 (8.0%)	4148 (4.7%)	2575 (3.8%)
	From 3XX	Urb_3	1464 (2.2%)	1217 (1.4%)	848 (1.3%)
	From 4XX/5XX	$Urb_{4,5}$	45 (0.1%)	62 (0.1%)	65 (0.1%)
All			66,194	87,763	67,473

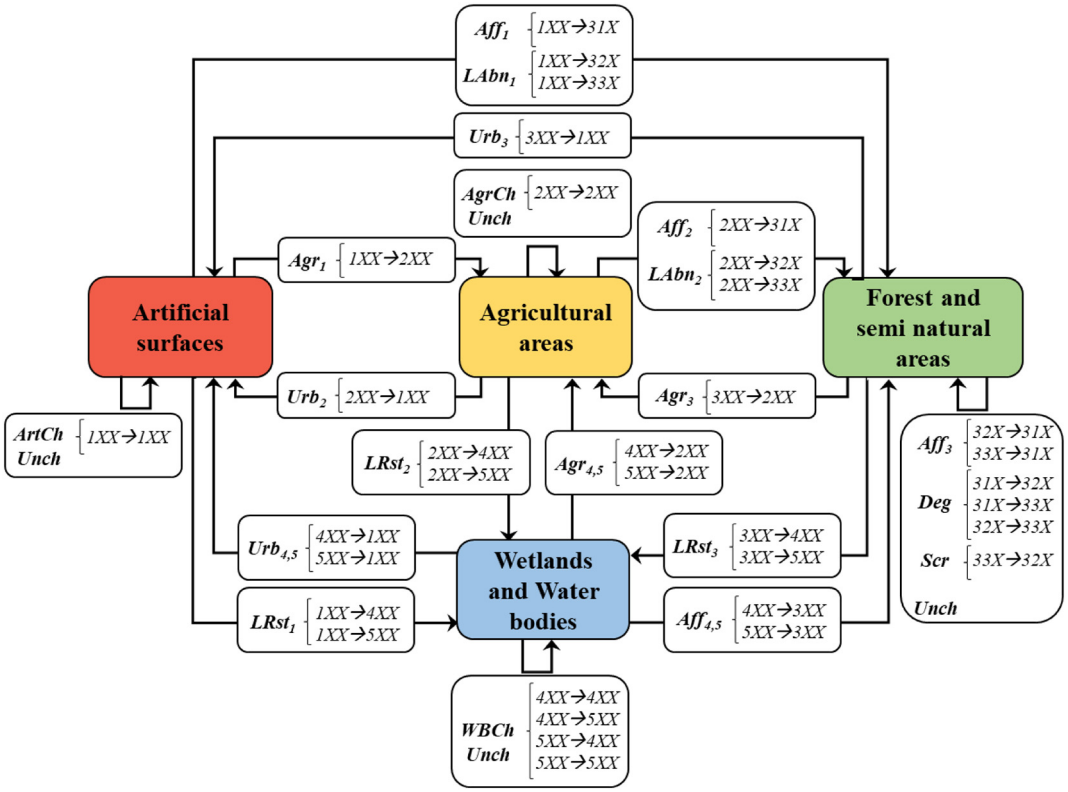

Fig. 2. Identification of the main land processes occurring in the territory based on the transitions observed between CLC products. Numerical subindices refer to the CLC Level1 category experiencing the land process. The format (XXX) in the white boxes refers to Level1, Level2 and Level3 CLC categories, respectively. (Aff: afforestation; Agr: agriculturalization; AgrCh: agricultural change; ArtCh: artificial use change; Deg: degradation; LAbn: land abandonment; LRst: land restoration; Scr: scrubland increase; Urb: urbanization; WBCh: wetlands and water bodies change; Unch: unchanged).

(Table 4), 2006-2012 (Table 5) and 2012-2018 (Table 6) temporal periods. Special attention was paid to the seasonal parameters that showed significant relationships in at least two of the three temporal periods (Figs. S1–S7). An example of land processes distribution (i.e. afforestation, agriculturalization, degradation, land abandonment and urbanization) obtained using Maximum seasonal parameter can be observed in Fig. 4.

3.2.1. Afforestation

Tables 4–6 show that the individual Afforestation processes (Aff_1, Aff_2, Aff_3 and $Aff_{4,5}$) could not be captured in the 3 temporal periods by any seasonality parameter. Aff1 was well characterized by Max in 2006-2012 and 2012-2018 (e.g. Fig. 4), but not in 2000-2006. During these periods, Max presented significant relationships (R^2 of 0.79-

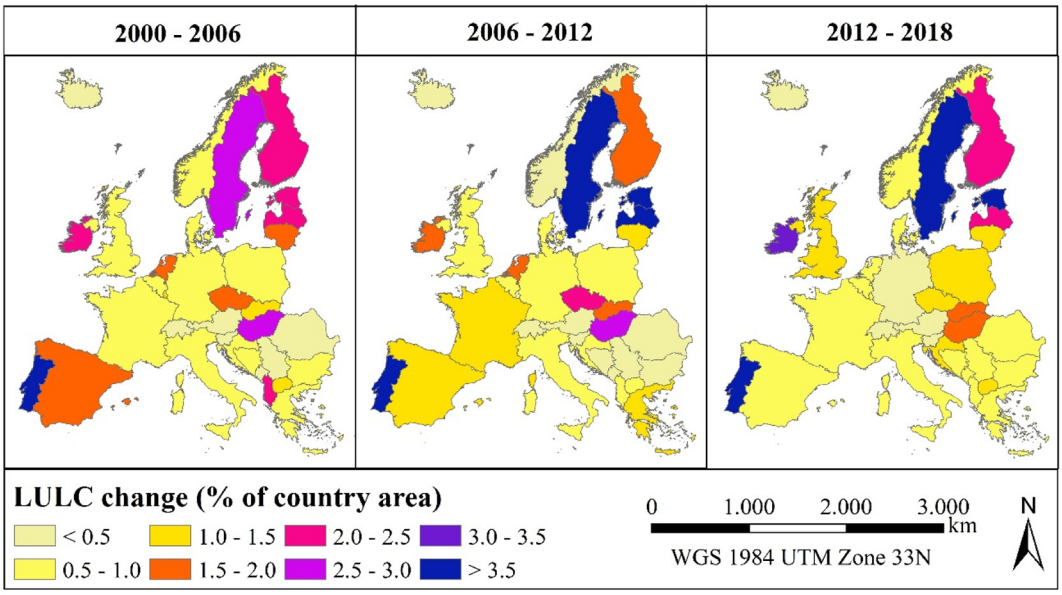

Fig. 3. Proportion of the territory affected by land use/land cover (LULC) changes for each country during the periods 2000-2006, 2006-2012 and 2012-2018 (expressed as % of the total country area).

Table 4
Equations, coefficients of determination and significances (*: p-value < 0.05; **: p-value < 0.01; ***: p-value < 0.001) of the temporal relationships obtained using the different seasonal parameters for each land process assessed during the period 2000–2006. Bold values indicate which of the significant relationships did not show significant differences between training and validating subsets.

	Ampl		Base		Lder		Length		Linteg		Max		Rder		Sinteg	
	Equation	R^2	Equation	R^2	Equation	R^2	Equation	R^2	Equation	R^2	Equation	R^2	Equation	R^2	Equation	R^2
Aff_1	−4.14 + 0.0022*X	0.04	**−25.17 + 0.0127*X**	**0.76***	−8.41 + 0.0042*X	0.59	−285.95 + 0.1510*X	0.15	**−609.93 + 0.3097*X**	**0.79***	−29.31 + 0.0150*X	0.62	19.17–0.0095*X	0.65	−11.67 + 0.0080*X	0.00
Aff_2	−2.76 + 0.0026*X	0.02	−24.60 + 0.0124*X	0.52	**−11.51 + 0.0058*X**	**0.83***	−319.58 + 0.1672*X	0.14	−499.40 + 0.2545*X	0.66	**−27.36 + 0.0140*X**	**0.96*****	10.23–0.0051*X	0.57	−0.37 + 0.0024*X	0.00
Aff_3	−0.81 + 0.0007*X	0.00	−6.61 + 0.0034*X	0.15	**−8.76 + 0.0044*X**	**0.86****	−21.44 + 0.0186*X	0.00	−153.75 + 0.0820*X	0.18	−7.42 + 0.0041*X	0.49	11.38–0.0056*X	0.61	−18.02 + 0.0124*X	0.00
$Aff_{4,5}$	**19.84–0.0098*X**	**0.69***	−8.33 + 0.0043*X	0.26	5.74–0.0028*X	0.55	−182.79 + 0.0982*X	0.27	−267.94 + 0.1373*X	0.51	11.51–0.0055*X	0.29	**3.75–0.0018*X**	**0.90****	109.70–0.0533*X	0.17
Agr_1	−18.60 + 0.0094*X	0.38	−6.60 + 0.0034*X	0.13	**−11.92 + 0.0060*X**	**0.93****	194.58–0.0894*X	0.04	−223.68 + 0.1156*X	0.26	**−25.20 + 0.0129*X**	**0.86****	3.37–0.0016*X	0.05	−166.88 + 0.0853*X	0.13
Agr_3	−2.26 + 0.0013*X	0.02	2.41–0.0011*X	0.05	−2.65 + 0.0014*X	0.16	214.59–0.0995*X	0.16	187.48–0.0896*X	0.12	0.15 + 0.0002*X	0.00	4.32–0.0021*X	0.20	78.92–0.0372*X	0.05
$Agr_{4,5}$	−11.05 + 0.0059*X	0.17	−0.52 + 0.0003*X	0.00	−5.43 + 0.0028*X	0.35	189.39–0.0870*X	0.08	71.05–0.0316*X	0.04	−11.56 + 0.0061*X	0.57	14.85–0.0073*X	0.36	44.54–0.0181*X	0.00
AgrCh	2.06–0.0008*X	0.01	−9.96 + 0.0051*X	0.27	**−9.77 + 0.0049*X**	**0.78***	209.66–0.0973*X	0.07	3.02 + 0.0024*X	0.00	−7.90 + 0.0042*X	0.36	11.07–0.0055*X	0.30	158.22–0.0767*X	0.12
ArtCh	1.58–0.0007*X	0.01	−0.20 + 0.0002*X	0.00	**−4.60 + 0.0023*X**	**0.90****	−138.63 + 0.0767*X	0.19	−86.92 + 0.0470*X	0.27	1.38–0.0004*X	0.05	5.16–0.0025*X	0.38	−19.10 + 0.0111*X	0.01
WBCh	−1.65 + 0.0010*X	0.02	−2.10 + 0.0011*X	0.02	−5.08 + 0.0026*X	0.17	102.88–0.0434*X	0.04	66.60–0.0306*X	0.09	−3.75 + 0.0021*X	0.10	−1.05 + 0.0006*X	0.04	50.65–0.0231*X	0.10
Deg	1.44–0.0005*X	0.00	13.04–0.0064*X	0.29	**−9.79 + 0.0049*X**	**0.80****	−120.51 + 0.0684*X	0.02	245.81–0.1176*X	0.35	**14.48–0.0069*X**	**0.68***	**12.61–0.0062*X**	**0.69***	25.57–0.0095*X	0.00
$LAbn_1$	−15.69 + 0.0080*X	0.30	−11.31 + 0.0057*X	0.26	**−14.13 + 0.0071*X**	**0.96****	434.72–0.2090*X	0.02	**−450.76 + 0.2290*X**	**0.70***	**−27.00 + 0.0137*X**	**0.89****	6.61–0.0033*X	0.20	−194.28 + 0.0991*X	0.14
$LAbn_2$	−0.48 + 0.0004*X	0.00	−2.85 + 0.0016*X	0.02	**−11.56 + 0.0058*X**	**0.74***	364.77–0.1742*X	0.19	51.36–0.0207*X	0.01	−3.34 + 0.0020*X	0.08	9.58–0.0047*X	0.26	109.42–0.0521*X	0.03
$LRst_1$	−4.95 + 0.0026*X	0.07	−2.84 + 0.0015*X	0.02	**−11.91 + 0.0060*X**	**0.80***	114.47–0.0495*X	0.13	−62.10 + 0.0342*X	0.09	−7.79 + 0.0041*X	0.45	7.19–0.0036*X	0.46	−7.95 + 0.0058*X	0.00
$LRst_2$	−2.70 + 0.0015*X	0.02	14.17–0.0070*X	0.36	**−5.99 + 0.0030*X**	**0.72***	94.75–0.0393*X	0.03	380.08–0.1857*X	0.65	11.46–0.0054*X	0.33	6.10–0.0030*X	0.17	95.57–0.0456*X	0.07
$LRst_3$	−7.96 + 0.0041*X	0.33	13.83–0.0069*X	0.58	**−7.41 + 0.0037*X**	**0.93****	−226.03 + 0.1203*X	0.02	**305.10–0.1495*X**	**0.70***	5.87–0.0027*X	0.17	4.43–0.0022*X	0.21	0.22 + 0.0022*X	0.00
Scr	−1.35 + 0.0008*X	0.01	−9.45 + 0.0049*X	0.65	−4.25 + 0.0021*X	0.43	189.43–0.0870*X	0.23	−342.43 + 0.1752*X	0.44	−10.80 + 0.0057*X	0.46	0.99–0.0005*X	0.01	−91.25 + 0.0468*X	0.14
Urb_2	9.48–0.0046*X	0.29	5.47–0.0026*X	0.10	**−4.94 + 0.0025*X**	**0.73***	55.93–0.0205*X	0.01	173.85–0.0828*X	0.59	**14.94–0.0072*X**	**0.89****	7.73–0.0038*X	0.59	113.34–0.0549*X	0.12
Urb_3	10.55–0.0051*X	0.34	14.05–0.0069*X	0.59	−2.72 + 0.0014*X	0.52	44.19–0.0145*X	0.01	**367.16–0.1793*X**	**0.74***	**24.60–0.0120*X**	**0.89****	**9.42–0.0047*X**	**0.69***	133.24–0.0645*X	0.19
$Urb_{4,5}$	15.59–0.0076*X	0.34	−9.70 + 0.0049*X	0.45	−0.82 + 0.0005*X	0.12	−632.81 + 0.3228*X	0.18	−64.03 + 0.0347*X	0.04	5.90–0.0027*X	0.18	**11.40–0.0056*X**	**0.70***	148.27–0.0715*X	0.08

Table 5
Equations, coefficients of determination and significances (*: p-value < 0.05; **: p-value < 0.01; ***: p-value < 0.001) of the temporal relationships obtained using the different seasonal parameters for each land process assessed during the period 2006–2012. Bold values indicate which of the significant relationships did not show significant differences between training and validating subsets.

	Ampl		Base		Lder		Length		Linteg		Max		Rder		Sinteg	
	Equation	R^2	Equation	R^2	Equation	R^2	Equation	R^2	Equation	R^2	Equation	R^2	Equation	R^2	Equation	R^2
Aff_1	**−35.79 + 0.0181*X**	**0.81****	2.91–0.0014*X	0.03	−2.40 + 0.0012*X	0.06	17.27–0.0004*X	0.00	**−394.96 + 0.2012*X**	**0.64***	−32.88 + 0.0167*X	0.97***	−4.45 + 0.0023*X	0.03	−440.55 + 0.2235*X	0.56
Aff_2	−24.94 + 0.0126*X	0.38	15.46–0.0075*X	0.23	−1.89 + 0.0010*X	0.04	−335.39 + 0.1748*X	0.33	−231.29 + 0.1203*X	0.35	−9.49 + 0.0051*X	0.44	−4.58 + 0.0023*X	0.10	−394.40 + 0.1987*X	0.42
Aff_3	−14.58 + 0.0076*X	0.31	13.50–0.0067*X	0.37	0.93–0.0004*X	0.02	−146.51 + 0.0808*X	0.13	−96.76 + 0.0531*X	0.12	−1.07 + 0.0009*X	0.09	1.53–0.0007*X	0.01	−299.08 + 0.1531*X	0.38
$Aff_{4,5}$	**−17.68 + 0.0090*X**	**0.67***	14.43–0.0072*X	0.51	0.50–0.0002*X	0.00	−15.43 + 0.0153*X	0.00	−133.98 + 0.0689*X	0.53	−3.25 + 0.0018*X	0.28	−2.23 + 0.0012*X	0.04	−323.36 + 0.1636*X	0.48
Agr_1	−24.57 + 0.0124*X	0.45	7.50–0.0036*X	0.06	−2.44 + 0.0012*X	0.10	−254.13 + 0.1340*X	0.18	**−336.02 + 0.1711*X**	**0.77****	**−17.07 + 0.0088*X**	**0.84****	−5.20 + 0.0026*X	0.12	−395.89 + 0.1989*X	0.40
Agr_3	−9.89 + 0.0051*X	0.42	6.58–0.0032*X	0.40	−0.78 + 0.0004*X	0.01	214.18–0.0993*X	0.44	113.61–0.0526*X	0.31	−3.32 + 0.0019*X	0.17	−2.75 + 0.0014*X	0.20	−82.06 + 0.0428*X	0.23
$Agr_{4,5}$	−16.06 + 0.0083*X	0.36	0.79–0.0004*X	0.00	1.95–0.0009*X	0.03	−129.96 + 0.0721*X	0.04	−148.97 + 0.0776*X	0.29	−15.27 + 0.0079*X	0.51	−5.72 + 0.0029*X	0.23	−226.62 + 0.1158*X	0.29
AgrCh	−19.38 + 0.0098*X	0.30	19.05–0.0094*X	0.28	0.48–0.0002*X	0.00	19.84–0.0024*X	0.00	21.88–0.0067*X	0.01	−0.33 + 0.0005*X	0.03	−4.17 + 0.0021*X	0.07	−321.02 + 0.1622*X	0.29
ArtCh	−12.23 + 0.0062*X	0.29	6.89–0.0033*X	0.11	−0.15 + 0.0001*X	0.00	10.78 + 0.0020*X	0.00	−62.30 + 0.0346*X	0.34	−5.34 + 0.0029*X	0.40	−3.30 + 0.0017*X	0.10	−184.76 + 0.0935*X	0.26
WBCh	−2.24 + 0.0013*X	0.01	12.81–0.0063*X	0.26	2.59–0.0012*X	0.04	9.43 + 0.0026*X	0.00	132.54–0.0629*X	0.22	**10.57–0.0050*X**	**0.94*****	−1.47 + 0.0008*X	0.02	−47.85 + 0.0261*X	0.01
Deg	−18.20 + 0.0093*X	0.40	**28.72–0.0142*X**	**0.66***	0.08 + 0.0000*X	0.00	−49.45 + 0.0326*X	0.03	177.14–0.0830*X	0.28	**10.52–0.0049*X**	**0.76***	−2.80 + 0.0015*X	0.04	−296.06 + 0.1508*X	0.48
$LAbn_1$	−32.93 + 0.0166*X	0.51	9.58–0.0047*X	0.09	−0.90 + 0.0005*X	0.01	−439.67 + 0.2266*X	0.36	**−435.35 + 0.2209*X**	**0.76***	**−23.35 + 0.0119*X**	**0.92*****	−6.90 + 0.0035*X	0.16	−507.73 + 0.2550*X	0.46
$LAbn_2$	−21.09 + 0.0107*X	0.22	21.21–0.0104*X	0.28	2.65–0.0013*X	0.02	−69.79 + 0.0428*X	0.02	−48.94 + 0.0294*X	0.04	0.11 + 0.0003*X	0.01	−6.26 + 0.0032*X	0.09	−363.27 + 0.1839*X	0.26
$LRst_1$	−28.40 + 0.0143*X	0.53	12.36–0.0061*X	0.17	−1.04 + 0.0006*X	0.01	−333.68 + 0.1738*X	0.17	−250.58 + 0.1283*X	0.49	**−16.04 + 0.0082*X**	**0.95*****	−5.50 + 0.0028*X	0.15	−366.44 + 0.1842*X	0.39
$LRst_2$	6.38–0.0030*X	0.13	**33.79–0.0168*X**	**0.65***	3.41–0.0017*X	0.32	**392.53–0.1887*X**	**0.72***	**597.33–0.2944*X**	**0.86****	**40.17–0.0198*X**	**0.78****	0.10 + 0.0000*X	0.00	63.91–0.0300*X	0.09
$LRst_3$	3.45–0.0016*X	0.12	**17.28–0.0086*X**	**0.72***	2.06–0.0010*X	0.25	**434.09–0.2088*X**	**0.59***	**362.64–0.1779*X**	**0.70***	**20.72–0.0101*X**	**0.66***	0.05 + 0.0000*X	0.00	46.96–0.0214*X	0.12
Scr	−2.66 + 0.0014*X	0.06	−7.39 + 0.0038*X	0.36	1.69–0.0008*X	0.11	336.62–0.1603*X	0.54	−108.05 + 0.0580*X	0.15	−10.05 + 0.0053*X	0.44	−1.42 + 0.0007*X	0.07	−12.56 + 0.0075*X	0.01
Urb_2	−3.17 + 0.0017*X	0.02	17.52–0.0086*X	0.31	2.56–0.0012*X	0.10	−11.16 + 0.0129*X	0.01	**211.84–0.1016*X**	**0.86****	**14.35–0.0069*X**	**0.79****	−1.36 + 0.0007*X	0.02	−102.50 + 0.0528*X	0.06
Urb_3	−0.38 + 0.0003*X	0.00	19.33–0.0095*X	0.60*	3.62–0.0018*X	0.23	0.00 + 0.0075*X	0.00	**290.65–0.1408*X**	**0.85****	**18.95–0.0092*X**	**0.78****	−0.24 + 0.0002*X	0.00	−37.70 + 0.0207*X	0.02
$Urb_{4,5}$	3.99–0.0018*X	0.02	14.39–0.0071*X	0.34	**8.60–0.0042*X**	**0.78****	−235.06 + 0.1243*X	0.11	218.66–0.1055*X	0.49	**18.38–0.0089*X**	**0.63***	8.05–0.0039*X	0.26	−29.87 + 0.0176*X	0.01

Table 6
Equations, coefficients of determination and significances (*: p-value < 0.05; **: p-value < 0.01; ***: p-value < 0.001) of the temporal relationships obtained using the different seasonal parameters for each land process assessed during the period 2012–2018. Bold values indicate which of the significant relationships did not show significant differences between training and validating subsets.

	Ampl		Base		Lder		Length		Linteg		Max		Rder		Sinteg	
	Equation	R^2	Equation	R^2	Equation	R^2	Equation	R^2	Equation	R^2	Equation	R^2	Equation	R^2	Equation	R^2
Aff_1	−6.72 + 0.0035*X	0.16	−9.41 + 0.0048*X	0.17	−2.42 + 0.0012*X	0.03	−296.44 + 0.1555*X	0.09	−516.76 + 0.2622*X	0.30	**−16.13 + 0.0084*X**	**0.79***	0.84–0.0004*X	0.00	−178.11 + 0.0908*X	0.11
Aff_2	8.16–0.0038*X	0.13	−23.60 + 0.0119*X	0.45	3.11–0.0015*X	0.12	−441.40 + 0.2270*X	0.59	**−606.39 + 0.3061*X**	**0.93****	−15.43 + 0.0080*X	0.55	−0.89 + 0.0005*X	0.01	−46.86 + 0.0258*X	0.02
Aff_3	**15.42–0.0073*X**	**0.71***	**−16.60 + 0.0083*X**	**0.80***	7.30–0.0036*X	0.30	−54.67 + 0.0353*X	0.03	−145.45 + 0.0775*X	0.18	−1.18 + 0.0010*X	0.04	−3.60 + 0.0019*X	0.09	160.52–0.0756*X	0.15
$Aff_{4,5}$	−6.80 + 0.0035*X	0.40	−9.18 + 0.0046*X	0.51	0.27–0.0001*X	0.00	694.48–0.3374*X	0.58	−191.47 + 0.0975*X	0.58	**−15.98 + 0.0081*X**	**0.97*****	−0.99 + 0.0005*X	0.06	28.22–0.0118*X	0.03
Agr_1	−4.93 + 0.0026*X	0.10	−18.43 + 0.0093*X	0.51	−1.93 + 0.0010*X	0.12	−252.90 + 0.1329*X	0.13	−454.81 + 0.2299*X	0.53	**−23.35 + 0.0119*X**	**0.75***	−0.31 + 0.0002*X	0.00	−93.82 + 0.0482*X	0.25
Agr_3	8.90–0.0042*X	0.45	1.17–0.0005*X	0.02	5.33–0.0026*X	0.30	116.25–0.0501*X	0.08	165.07–0.0774*X	0.26	10.07–0.0047*X	0.62	1.82–0.0009*X	0.06	125.77–0.0599*X	0.33
$Agr_{4,5}$	4.46–0.0019*X	0.02	**−19.73 + 0.0099*X**	**0.80***	0.29–0.0001*X	0.00	−159.96 + 0.0868*X	0.17	−258.50 + 0.1326*X	0.38	−15.27 + 0.0079*X	0.42	3.27–0.0016*X	0.11	93.96–0.0437*X	0.04
AgrCh	11.22–0.0054*X	0.30	−2.56 + 0.0014*X	0.03	5.82–0.0029*X	0.37	−78.86 + 0.0463*X	0.08	−71.39 + 0.0397*X	0.17	**8.66–0.0040*X**	**0.92****	1.76–0.0008*X	0.02	56.03–0.0256*X	0.10
ArtCh	3.04–0.0014*X	0.04	−10.54 + 0.0054*X	0.26	1.73–0.0008*X	0.06	−5.48 + 0.0102*X	0.02	−183.15 + 0.0951*X	0.53	−7.50 + 0.0040*X	0.65	0.73–0.0003*X	0.01	9.47–0.0030*X	0.00
WBCh	3.79–0.0017*X	0.04	**13.03–0.0064*X**	**0.85****	1.53–0.0007*X	0.04	−242.58 + 0.1283*X	0.32	229.61–0.1099*X	0.20	16.82–0.0081*X	0.46	2.47–0.0012*X	0.10	81.65–0.0382*X	0.07
Deg	**17.96–0.0087*X**	**0.80***	−3.73 + 0.0020*X	0.14	6.22–0.0030*X	0.28	148.67–0.0657*X	0.08	186.55–0.0872*X	0.17	**14.23–0.0067*X**	**0.67***	1.66–0.0008*X	0.04	274.01–0.1326*X	0.48
$LAbn_1$	−8.16 + 0.0042*X	0.49	**−15.30 + 0.0077*X**	**0.69***	2.10–0.0010*X	0.10	−238.66 + 0.1264*X	0.31	−448.20 + 0.2269*X	0.61	**−23.46 + 0.0119*X**	**0.85****	0.13 + 0.0000*X	0.00	−156.84 + 0.0804*X	0.45
$LAbn_2$	7.06–0.0033*X	0.09	−12.27 + 0.0062*X	0.21	5.65–0.0028*X	0.19	−255.23 + 0.1347*X	0.28	−288.98 + 0.1488*X	0.39	−5.21 + 0.0029*X	0.56	1.84–0.0009*X	0.02	2.16 + 0.0015*X	0.00
$LRst_1$	−6.33 + 0.0033*X	0.10	−11.93 + 0.0061*X	0.31	0.19–0.0001*X	0.00	−191.71 + 0.1031*X	0.12	−481.47 + 0.2434*X	0.65	−18.26 + 0.0094*X	0.86**	0.65–0.0003*X	0.01	−124.94 + 0.0640*X	0.22
$LRst_2$	13.74–0.0067*X	0.39	7.84–0.0038*X	0.59	3.77–0.0018*X	0.32	**−244.31 + 0.1289*X**	**0.66***	98.20–0.0045*X	0.27	**21.58–0.0104*X**	**0.68***	3.60–0.0018*X	0.37	73.22–0.0344*X	0.22
$LRst_3$	12.66–0.0060*X	0.50	−1.39 + 0.0007*X	0.08	5.42–0.0026*X	0.21	−122.34 + 0.0688*X	0.06	139.74–0.0659*X	0.13	11.28–0.0053*X	0.39	−0.25 + 0.0002*X	0.00	158.21–0.0748*X	0.14
Scr	0.61–0.0001*X	0.00	−16.45 + 0.0083*X	0.54	−0.30 + 0.0002*X	0.00	227.07–0.1049*X	0.11	−203.29 + 0.1056*X	0.11	−15.84 + 0.0082*X	0.41	1.46–0.0007*X	0.06	5.47–0.0007*X	0.00
Urb_2	13.45–0.0065*X	0.35	−0.71 + 0.0005*X	0.00	4.66–0.0023*X	0.24	**−231.74 + 0.1224*X**	**0.71***	−19.00 + 0.0138*X	0.02	**12.73–0.0060*X**	**0.67***	3.31–0.0016*X	0.17	77.37–0.0366*X	0.08
Urb_3	**24.17–0.0118*X**	**0.85****	−1.26 + 0.0007*X	0.04	5.85–0.0029*X	0.22	102.00–0.0427*X	0.05	352.24–0.1702*X	0.62	**22.91–0.0111*X**	**0.92****	**5.57–0.0027*X**	**0.70***	**319.52–0.1560*X**	**0.76***
$Urb_{4,5}$	20.52–0.0100*X	0.56	−5.24 + 0.0027*X	0.09	3.17–0.0015*X	0.16	345.21–0.1635*X	0.13	347.90–0.1687*X	0.52	15.28–0.0073*X	0.55	−0.68 + 0.0004*X	0.01	326.24–0.1591*X	0.34

0.97), with positive slopes (0.0084-0.0167) and initial and final Max values for each period ranging from 0.65 to 0.69, and 0.74 to 0.75, respectively. For this seasonal parameter, significant differences were found for 2006-2012 between the relationships obtained during the training and validation process (Table 5). Additionally, Linteg obtained significant relationships for Aff_1 in 2000-2006 and 2006-2012 (R^2 of 0.64-0.79), with positive slopes (0.2012-0.3097) and Linteg values at the beginning and at the end of the periods varying from 8.72 to 9.43 and 9.93 to 11.29, respectively. However, Linteg did not present a significant relationship for Aff_1 for the period 2012-2018 (Table 6). Regarding $Aff_{4,5}$, amplitude was the seasonal parameter that better related with this land process, showing significant relationships for the 2000-2006 and 2006-2012 time-periods (R^2 0.67-0.69). Nevertheless, the obtained slopes presented different sign for each period (negative in 2000-2006 and positive in 2006-2012) and the initial and final Amplitude values ranged from 0.28 to 0.38 and from 0.22 to 0.44, respectively. For Aff_2 and Aff_3, no seasonality parameter was able to evidence these land processes except for a single temporal period (e.g. Lder for 2000-2006; Table 4).

3.2.2. Agriculturalization

For the agriculturalization process (Fig. 4), Max parameter showed significant relationships during the three studied periods (R^2 from 0.75 to 0.86; Tables 4–6), but only when this process occurred on urban categories (i.e. Agr_1). The slope of these significant relationships was always positive and ranged from 0.0088 (in 2006-2012) to 0.0129 (in 2012-2018), whereas the Max values at the beginning and at the end of each period varied from 0.50 to 0.53 and from 0.56 to 0.60, respectively (Tables 4–6). Some other seasonal parameters (e.g. Base in 2012-2018, Lder in 2000-2006 and Linteg in 2006-2012; Tables 4–6) showed sporadic significant relationships during a single period in Agr_1 and $Agr_{4,5}$; whereas no seasonal parameter was able to identify Agr_3 in any studied period (Tables 4–6).

3.2.3. Degradation

Land degradation process showed sensitive to changes in Max seasonal parameter in the three temporal periods evaluated (Fig. 4). The slope of these significant relationships (R^2 ranging from 0.67 to 0.76), was negative and oscillated between -0.0049 and -0.0069 (Tables 4–6). The initial and final Max values for each period ranged from 0.73 to 0.75 and from 0.69 to 0.71 (Tables 4–6). Contrarily, Ampl, Base, Lder and Rder seasonal parameters were only able to occasionally capture Deg in one of the three evaluated periods.

3.2.4. Intra-class changes

Changes occurred within the same CLC level 1 category (i.e. AgrCh, ArtCh and WBCh) were not reflected by any seasonal parameter, rather than in any specific period where significant relationships were obtained (e.g. Lder for AgrCh and ArtCh in 2000-2006) that were not recurrent in the other periods (Tables 4–6).

3.2.5. Land abandonment

Land abandonment processes occurring in urban classes (i.e. $LAbn_1$) were well-captured by Max seasonality parameter in the three assessed temporal periods (Fig. 4), showing significant relationships (R^2 of 0.85-0.92) with positive slopes ranging from 0.0119 to 0.0137 (Tables 4–6). The Max values at the beginning and at the end of the temporal periods oscillated between 0.48 and 0.58; and between 0.56 and 0.65, respectively. Moreover, Land Abandonment processes occurring in urban classes (i.e. $LAbn_1$) was accurately characterized by Linteg, but in this case in two of the three evaluated periods (2000-2006 with a R^2 of 0.70; and 2006-2012 with a R^2 value of 0.76). In these two periods, the significant relationships obtained for Linteg were characterized by positive slopes (0.2209-0.2290) and initial and final Linteg values of 7.30-7.73 and 8.67-9.05, respectively (Tables 4–5). It has to be noted that the period 2012-2018, despite not being statistically significant, presented a relationship with similar slope, initial and final values than those obtained for 2000-

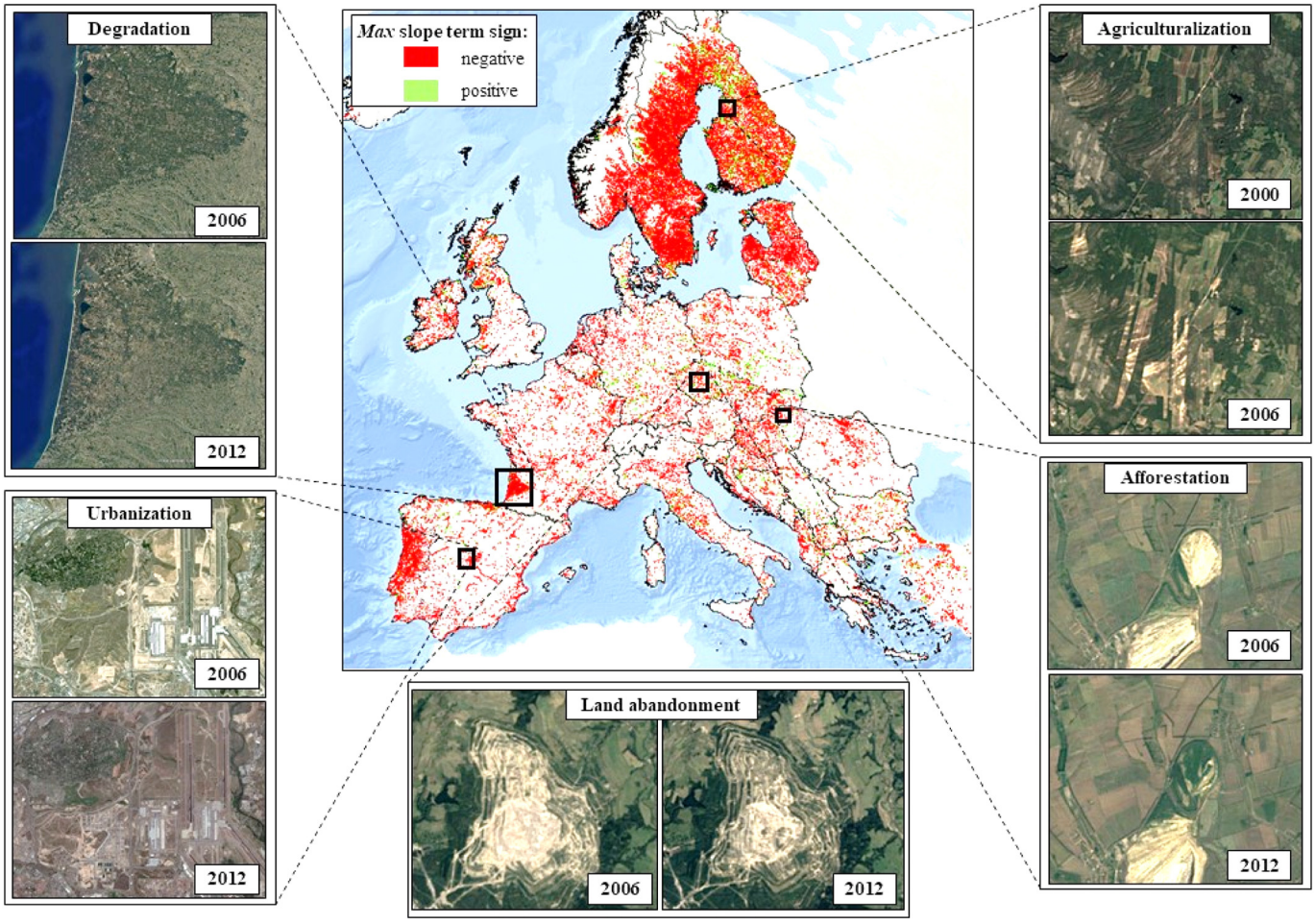

Fig. 4. Land processes distribution obtained through the evaluation of the magnitude and sign of the slope term of the Maximum seasonal parameter.

2006 and 2006-2012 (Table 6). Land abandonment of previously cultivated areas (i.e. $LAbn_2$) could not be significantly captured by any seasonal parameter with the exception of Lder in the period 2000-2006 (Table 4).

3.2.6. Land restoration

Similarly to what reported for Afforestation and Intra-class changes processes, there were not seasonal parameters able to detect Land Restoration process during the three evaluated period. However, significant relationships were found with some of them in two of the three periods. Specifically, Linteg was sensitive to $LRst_3$ for the periods 2000-2006 and 2006-2012 (R^2 of 0.70 for both periods), having negative slopes (-0.1779- -0.1495) and initial and final Linteg values of 5.74-6.19 and 4.68-5.30, respectively. $LRst_1$ presented significant relationships with Max for the periods 2006-2012 and 2012-2018 (R^2 of 0.95 and 0.86, respectively). In this case, the obtained slopes were positive (0.0082-0.0094) and the Max values at the beginning and at the end of the periods ranged from 0.47 to 0.56 and from 0.52 to 0.61, respectively. Nevertheless, significant differences were found for 2012-2018 between the relationships obtained for Max seasonal parameter during the training and validation process (Table 6). Regarding $LRst_2$, Length (R^2 of 0.66-0.72) and Max (R^2 of 0.68-0.78) showed significant relationships for the periods 2006-2012 and 2012-2018. From the Length relationship, it can be noted that opposite sign slopes were obtained for each of the periods (-0.1887 for 2006-2012 and 0.1289 for 2012-2018) whereas the initial and final Length values were 13.99 and 15.05 for 2006-2012; and 12.86 and 15.82 for 2012-2018, respectively. On the other hand, Max significant relationships presented negative slopes (from -0.0104 to -0.0198) and initial and final Max values for each period ranging from 0.53 to 0.62, and 0.41 to 0.55, respectively.

3.2.7. Scrubland increase

The land process referring to scrubland increase did not present significant relationships with any seasonal parameter, not even in a sporadic temporal period as happened with the other land processes (Tables 4–6). The lack of significance was also evidenced by the low R^2 values derived from the assessed relationships, with a mean R^2 of 0.22, being lower than 0.65 in all cases (Tables 4–6).

3.2.8. Urbanization

Urbanization, specifically Urb_2 and Urb_3, showed significant relationships with the temporal evolution of Max for the three considered temporal periods (R^2 ranging from 0.67 to 0.89 for Urb_2 and from 0.78 to 0.92 for Urb_3). Both Urb_2 and Urb_3 obtained negative slopes, being slightly steeper for Urb_3 than for Urb_2 (-0.006 - -0.007 for Urb_2 versus -0.091 - -0.012 for Urb_3). However, the Max values at the beginning and at the end of the periods obtained for Urb_2 and Urb_3 were quite similar, ranging from 0.56 to 0.66 and from 0.50 to 0.59, respectively. Moreover, Urb_3 presented also significant relationships for Linteg (R^2 of 0.74-0.85) and Rder (R^2 of 0.69-0.70) for two of the three considered periods (2000-2006 and 2006-2012 for Linteg; and 2000-2006 and 2012-2018 for Rder). The slopes for the Linteg relationships ranged from -0.1408 to -0.1793 with initial and final values for each period of 8.11-8.54 and 7.27-7.47, respectively. Concerning the Rder relationships, their slopes varied from 0.0027 to 0.0047 and the initial and final values for each season from 0.09 to 0.11 and from 0.07 to 0.10 respectively. On the contrary, $Urb_{4,5}$ could not be significantly detected in more than one period as, for instance, Lder and Max in the period 2006-2012 and Rder in the period 2000-2006.

4. Discussion

The use of time-series change detection methods, such as TIMESAT, overcomes some of the limitations of post-classification change detection approaches. Specifically, they consider the continuity of time-series changes avoiding obtaining two relatively isolated classifications for each single acquisition period (Yan et al., 2019). However, they are subjected to a series of shortcomings, mainly related to the inefficacy in detecting frequent and subtle changes (Jamali et al., 2015; Cai and Liu, 2015; Zhu et al., 2019) and to the high demand of computational resources (Zhu et al., 2019; Zhu and Woodcock, 2014).

Direct application of vegetation indexes derived from remote sensing (e.g. NDVI) for identifying LULC seasonal patterns is limited by the high degree of noise in the data as consequence of variable atmospheric conditions and sun-sensor-surface viewing geometries at the moment of the image acquisition (Ma and Veroustraete, 2006; Hird and McDermid, 2009, Atkinson et al., 2012). Thus, the use of fitted functions helps to reduce the intrinsic uncertainties while maintaining the relevant NDVI signal integrity leading to more robust determinations. In this sense, Hird and McDermid (2009) compared six NDVI time series noise-reduction techniques concluding that the asymmetric Gaussian and double logistic function-fitting techniques achieved the highest performance. These findings are in line with the conclusions drawn by other studies, which showed the robustness of double logistic function for phenological parameter estimation under a variety of conditions (Jönsson and Eklundh, 2002, 2004; Cai et al., 2017; Jönsson et al., 2018; Vanella et al., 2020). Additionally, Michishita et al. (2014) also observed noise reductions using asymmetric Gaussian and double logistic function-fitting techniques. However, these authors obtained the most remarkably noise reductions using Running Median, Mean value, maximum operation, End point processing, and Hanning smoothing (Jin and Xu, 2013) and the iterative Savitzky–Golay (Chen et al., 2004) filters, indicating that function-fitting techniques performance depends on the land cover types and the study area. Due to these previous researches and the general nature of the land-use change phenomena to be characterized in this study, the double logistic function was used. This is despite that for the characterization of some specific LULC changes, especially those involving more abrupt changes, other fitting functions would be preferable (Jönsson and Eklundh, 2002). Additionally, this study assumes that LULC processes follow a linear behaviour, which could not represent the non-linear trend of the natural systems (Barbier et al., 2008). To solve these limitations, instead of analysing the entire period as a whole (2000-2018), the approach followed in the present study considered shorter temporal periods, thus discretizing a long non-linear process into multiple shorter linear segments (i.e. 2000-2006, 2006-2012 and 2012-2018).

The LULC change identification process performed has demonstrated that certain degree of classification details (as those provided by CLC Levels 2 and 3) are needed for a proper detection of land processes. If coarser classifications are used (e.g. CLC Level1) the recognition of some phenomena could be hidden due to the different patterns that internal sub-classes have. The assessment of the slope term allowed for the identification of the LULC intensity, which is quite dependent of the initial and final status (i.e. the initial and final NDVI-related seasonal parameters values). In this sense, there was not a unique period in which all LULC processes were more intense, but it depended also on the LULC process itself. For instance, analysing the slope obtained for Max seasonal parameter, the intensity of the afforestation process (Aff_1) was higher during 2006-2012 than during 2006-2012. However, agriculturalization (Agr_1), degradation (Deg) and land abandonment ($LAbn_1$) processes were more pronounced in the first period (2000-2006) than in 2006-2012 and 2012-2018. The intensity of the change depended also on the initial and the final status. Although a LULC process is identified in multiple pixels, it could be that several pixels with the same LULC started from different conditions and/or finished in different change status. (represented by the initial and final values). The fraction of the pixel affected by a LULC process also influenced the obtained relationships. For instance, urbanization affecting 75% of the pixel will be better identified than urbanization when affecting to a smaller pixel proportion. This could be solved by using better spatial resolution LULC products, as for instance those generated from unmanned aerial vehicles, which agree with previous findings (Eckert et al., 2015; Ovejero-Campos et al., 2019). These authors pointed out the spatial resolution as one of the main limitations of using CLC for assessing land cover changes. Another limitation of the methodology used in this study is that it did not allow detecting LULC changes occurring inside the same CLC Level1 category. Specifically, these processes refer to AgrCh, ArtCh and WBCh. This is because the initial and final LULC categories involved in the process have similar temporal patterns in terms of NDVI, and thus, in terms of the seasonal parameter. In this sense, the evaluation of alternative terrain characteristics, as the surface roughness by using radar images; could help their identification. An example of this is found in Sica et al. (2019), who used SAR interferometry from Sentinel 1 imagery for LULC classification over central Europe.

In this study, transitions among LULC were better characterized by the maximum seasonal parameter. Specifically, afforestation, agriculturalization, land abandonment and land restoration processes were characterized by a positive Max trend representing the increase in vegetation from the initial to the final LULC involved in the land processes (Estel et al., 2015; Zhang and Roy, 2017). On the contrary, degradation and urbanization are represented by negative Max patterns as expected in surfaces, which lose vegetation fraction in favour of less-vegetated surfaces (e.g. anthropic areas; Esau et al., 2016). Generally, maximum NDVI values (and therefore Max seasonal parameter) coincide with the emergence of spontaneous ground cover, which usually develops on natural/agricultural areas (Estel et al., 2015). This could explain also the lack of sensibility of other seasonal parameters, as for instance the base value, that usually take place when the surface is without natural ground cover or the vegetation without foliage (e.g. for deciduous vegetation; Yang et al., 2017). Therefore, natural vegetation cover monitoring could be used as an indirect indicator for the identification of land processes. Moreover, the better performances of Max when compared with Sinteg and Linteg suggest that some land processes are better identified at specific moment of the season, whereas its identification could be hindered when considering the entire season, as Sinteg and Linteg do.

In addition, it is important to highlight that a more precise characterization of the seasonal parameter patterns could be reached through a more detailed classification of the different LULCs. It can be achieved, for instance, by using a CLC-level able to distinguish between evergreen and deciduous forests or even between different species; or a higher resolution imagery that reduce land processes contamination within a pixel. Moreover, abiotic/biotic stresses could directly affect VI values (Vanella et al., 2020), which if taken into account, may also contribute to further improve land processes characterization.

The significant discrepancies observed between the results obtained with the training and validation dataset when analysing some LULC processes (e.g. Aff_1 and $LRst_1$ with Max for the period 2006-2012 and 2012-2018, respectively; and Urb_3 with Base for 2006-2012) are explained by the small surface affected by these processes (ranging from 22 to 89 km^2 for the previous examples; Table 3). This behaviour has been evidenced by Xu and Goodacre (2018), who found that the size of the data was the deciding factor for the quality performance of the training and validation procedures, indicating that the discrepancies among them decreased when a higher number of samples were available.

Given the suitability of this methodology for characterizing LULC processes, it could be combined with other classification methods for improving LULC detection accuracy.

In this sense, results derived from this study could be incorporated into a multi-criteria or rule based decision tree classification, where different thresholds in terms of slope and initial and final seasonal parameter values are used for discriminating LULC processes.

The use of this approach will allow identifying LULC processes in locations where no LULC maps are available, improving their spatial

resolution, regularly updating LULC maps, or identifying these processes in a shorter temporal resolution (e.g. a specific moment between two CORINE LULC maps). This is especially relevant for areas where terrestrial ecosystems are threatened by food security, biodiversity loss, and climate change (e.g. Africa continent, Xu et al., 2019). Additionally, such information can be used by policy-makers to draw LULC management actions associated with the United Nations sustainable development goals, as it has been highlighted by other studies (Theobald et al., 2005; Koomen et al., 2008; Mustaphi et al., 2019; Duveiller et al., 2020). Analysing the spatial patterns for changes in LULC can help to highlight hot spots where additional pressure on natural resources exploitation is occurring or might be exacerbated in the near future. This is particularly relevant for land and water conservation studies where actions to implement preservation measures are more urgent. In addition, methods as proposed here for assessing LULC changes could be useful for harmonising the tools to be used for the proper assessment and monitoring of land degradation and suggesting tailored site-specific solutions involving using multi-criteria methods. The possibility of determining temporal pattern in LULC at large scale can also help to better integrate, in a given large area, the availability of resources and current LULC. This approach could be useful for instance for a more quantitative assessment of the water-food-energy nexus considering different scenarios for LULC.

5. Conclusions

A seasonal parameter-based procedure was assessed and validated for characterizing main land processes occurring at European level during the period 2000-2018. CLC inventories for the years 2000, 2006, 2012 and 2018 were taken as basin for identifying the relationships between the LULC transitions and the seasonal parameters determined from MODIS NDVI time-series. The main key points derived from this work can be summarized as in the follows:

- The temporal evolution of the maximum NDVI value was the seasonal parameter that better characterized the occurrence of most of the land processes evaluated.
- Linteg also presented significant relationships but they were restricted to two of the three evaluated periods.
- Land processes involving CLC categories with similar NDVI patterns were not well captured with the proposed methodology (e.g. AgrCh, ArtCh, WBCh and Scr).

CRediT authorship contribution statement

J.M. Ramírez-Cuesta: Conceptualization, Methodology, Validation, Formal analysis, Writing – original draft. **M. Minacapilli:** Conceptualization, Methodology, Writing – review & editing. **A. Motisi:** Methodology, Data curation, Writing – review & editing. **S. Consoli:** Writing – review & editing, Supervision. **D.S. Intrigliolo:** Writing – review & editing, Supervision, Funding acquisition. **D. Vanella:** Conceptualization, Methodology, Validation, Writing – original draft, Visualization, Supervision.

Declaration of competing interest

The authors declare that they have no known competing financial interests or personal relationships that could have appeared to influence the work reported in this paper.

Acknowledgments

The research is supported by European Union H2020 project SHUI GA 773903. J.M. Ramirez-Cuesta acknowledges the postdoctoral financial support received from Juan de la Cierva Spanish Postdoctoral Program (FJC2018-037196-I).

Appendix A. Supplementary data

Supplementary data to this article can be found online at https://doi.org/10.1016/j.scitotenv.2021.149346.

References

Ackerman, S., Strabala, K., Menzel, P., Frey, R., Moeller, C., Gumley, L., Baum, B., Schaaf, C., Riggs, G., Welch, R., 1996. Discriminating clear-sky from cloud with MODIS algorithm theoretical basis document V3. http://eospso.gsfc.nasa.gov/atbd/modistables.html.

Atkinson, P.M., Jeganathan, C., Dash, J., Atzberger, C., 2012. Inter-comparison of four models for smoothing satellite sensor time-series data to estimate vegetation phenology. Remote Sens. Environ. 123, 400–417.

Barbier, E.B., Koch, E.W., Silliman, B.R., Hacker, S.D., Wolanski, E., Primavera, J.H., Granek, E.F., Polasky, S., Aswani, S., Stoms, D.M., Kennedy, C.J., Bael, D., Kappel, C.V., Perillo, G.M., Reed, D.J., Cramer, L.A., 2008. Coastal ecosystem-based management with nonlinear ecological functions and values. Science 319, 321–323.

Bradley, B.A., Jacob, R.W., Hermance, J.F., Mustard, J.F., 2007. A curve fitting procedure to derive inter-annual phenologies from time series of noisy satellite NDVI data. Remote Sens. Environ. 106, 137–145.

Cai, S., Liu, D., 2015. Detecting change dates from dense satellite time series using a subannual change detection algorithm. Remote Sens. 7, 8705–8727.

Cai, Z., Jönsson, P., Jin, H., Eklundh, L., 2017. Performance of smoothing methods for reconstructing NDVI time-series and estimating vegetation phenology from MODIS data. Remote Sens. 9, 1271.

Chen, J., Jönsson, P., Tamura, M., Gu, Z., Matsushita, B., Eklundh, L., 2004. A simple method for reconstructing a high-quality NDVI time-series data set based on the savitzky-golay filter. Remote Sens. Environ. 91, 332–344.

Chen, B., Huang, B., Xu, B., 2017. Multi-source remotely sensed data fusion for improving land cover classification. ISPRS J. Photogramm. Remote Sens. 124, 27–39.

Didan, K., 2015. MOD13A2 MODIS/Terra Vegetation Indices 16-Day L3 Global 1km SIN Grid V006. NASA EOSDIS Land Processes DAAC https://doi.org/10.5067/MODIS/MOD13A2.006.

Didan, K., Munoz, A.B., Solano, R., Huete, A., 2015. MODIS Vegetation Index User's Guide (MOD13 Series). University of Arizona, Vegetation Index and Phenology Lab.

Di Gregorio, M., Fatorelli, L., Paavola, J., Locatelli, B., Pramova, E., Nurrochmat, D.R., May, P.H., Brockhaus, M., Sari, I.M., Kusumadewi, S.D., 2019. Multi-level governance and power in climate change policy networks. Glob. Environ. Chang. 54, 64–77.

Duveiller, G., Caporaso, L., Abad-Viñas, R., Perugini, L., Grassi, G., Arneth, A., Cescatti, A., 2020. Local biophysical effects of land use and land cover change: towards an assessment tool for policy makers. Land Use Policy 91, 104382.

Eckert, S., Hüsler, F., Liniger, H., Hodel, E., 2015. Trend analysis of MODIS NDVI time series for detecting land degradation and regeneration in Mongolia. J. Arid Environ. 113, 16–28.

Eklundh, L., Jönsson, P., 2017. TIMESAT 3.3 Software Manual. Lund and Malmö University, Sweden. In: Maxwell, J. Clerk (Ed.), A Treatise on Electricity and Magnetism, 3rd ed. 2. Clarendon, Oxford, pp. 68–73 1892.

Esau, I., Miles, V.V., Davy, R., Miles, M.W., Kurchatova, A., 2016. Trends in normalized difference vegetation index (NDVI) associated with urban development in northern West Siberia. Atmos. Chem. Phys. 16, 9563–9577.

Estel, S., Kuemmerle, T., Alcantara, C., Levers, C., Prishchepov, A.V., Hostert, P., 2015. Mapping farmland abandonment and recultivation across Europe using MODIS NDVI time series. Remote Sens. Environ. 163, 312–325.

Foley, J.A., DeFries, R., Asner, G.P., Barford, C., Bonan, G., Carpenter, S.R., Chapin, F.S., Coe, M.T., Daily, G.C., Gibbs, H.K., Helkowski, J.H., Holloway, T., Howard, E.A., Kucharik, C.J., Monfreda, C., Patz, J.A., Prentice, I.C., Ramankutty, N., Snyder, P.K., 2005. Global consequences of land use. Science 309, 570–574.

Gholamnia, M., Khandan, R., Bonafoni, S., Sadeghi, A., 2019. Spatiotemporal analysis of MODIS NDVI in the semi-arid region of Kurdistan (Iran). Remote Sens. 11, 1723.

Gómez-Mendoza, L., Vega-Peña, E., Ramírez, M.I., Palacio-Prieto, J.L., Galicia, L., 2006. Projecting land-use change processes in the Sierra Norte of Oaxaca, Mexico. Appl. Geogr. 26, 276–290.

Grimm, N.B., Faeth, S.H., Golubiewski, N.E., Redman, C.L., Wu, J.G., Bai, X.M., Briggs, J.M., 2008. Global change and the ecology of cities. Science 319, 756–760.

Hird, J.N., McDermid, G.J., 2009. Noise reduction of NDVI time series: an empirical comparison of selected techniques. Remote Sens. Environ. 113, 248–258.

Huete, A., Justice, C., Van Leeuwen, W., 1999. MODIS vegetation index (MOD13). Algorithm Theoretical Basis Document. 3, p. 213.

IPCC, 2019. Summary for policymakers. In: Shukla, P.R., Skea, J., Buendia, E. Calvo, Masson-Delmotte, V., Roberts, D.C., Zhai, P., Slade, R., Connors, S., van Diemen, R., Ferrat, M., Haughey, E., Luz, S., Neogi, S., Pathak, M., Petzold, J., Pereira, J. Portugal, Vyas, P., Huntley, E., Kissick, K., Belkacemi, M., Malley, J., Pörtner, H.-O. (Eds.), Climate Change and Land: An IPCC Special Report on Climate Change, Desertification, Land Degradation, Sustainable Land Management, Food Security, and greenhouse gas fluxes in terrestrial ecosystems In press.

Jamali, S., Jönsson, P., Eklundh, L., Ardö, J., Seaquist, J., 2015. Detecting changes in vegetation trends using time series segmentation. Remote Sens. Environ. 156, 182–195.

Jia, K., Liang, S., Wei, X., Yao, Y., Su, Y., Jiang, B., Wang, X., 2014. Land cover classification of Landsat data with phenological features extracted from time series MODIS NDVI data. Remote Sens. 6, 11518–11532.

Jin, Z., Xu, B., 2013. A novel compound smoother – RMMEH to reconstruct MODIS NDVI time series. IEEE Geosci. Remote Sens. Lett. 10, 942–946.

Jönsson, P., Eklundh, L., 2002. Seasonality extraction and noise removal by function fitting to time-series of satellite sensor data. IEEE Trans. Geosci. Remote Sens. 40, 1824–1832.
Jönsson, P., Eklundh, L., 2004. TIMESAT—a program for analyzing time-series of satellite sensor data. Comput. Geosci. 30, 833–845.
Jönsson, P., Cai, Z., Melaas, E., Friedl, M.A., Eklundh, L., 2018. A method for robust estimation of vegetation seasonality from Landsat and Sentinel-2 time series data. Remote Sens. 10, 635.
Kennedy, R.E., Cohen, W.B., Schroeder, T.A., 2007. Trajectory-based change detection for automated characterization of forest disturbance dynamics. Remote Sens. Environ. 110, 370–386.
Koomen, E., Rietveld, P., de Nijs, T., 2008. Modelling land-use change for spatial planning support. Ann. Reg. Sci. 42, 1–10.
Kosztra, B., Büttner, G., Hazeu, G., Arnold, S., 2017. Updated CLC Illustrated Nomenclature Guidelines. European Environment Agency, Copenhagen, Denmark.
Lasanta, T., Vicente-Serrano, S.M., 2012. Complex land cover change processes in semiarid Mediterranean regions: an approach using Landsat images in Northeast Spain. Remote Sens. Environ. 124, 1–14.
Levers, C., Schneider, M., Prishchepov, A.V., Estel, S., Kuemmerle, T., 2018. Spatial variation in determinants of agricultural land abandonment in Europe. Sci. Total Environ. 644, 95–111.
Luo, Y., Lü, Y., Liu, L., Liang, H., Li, T., Ren, Y., 2020. Spatiotemporal scale and integrative methods matter for quantifying the driving forces of land cover change. Sci. Total Environ. 739, 139622.
Lu, L., Weng, Q., Guo, H., Feng, S., Li, Q., 2019. Assessment of urban environmental change using multi-source remote sensing time series (2000–2016): a comparative analysis in selected megacities in Eurasia. Sci. Total Environ. 684, 567–577.
Ma, M., Veroustraete, F., 2006. Reconstructing pathfinder AVHRR land NDVI time-series data for the Northwest of China. Adv. Space Res. 37 (4), 835–840. https://doi.org/10.1016/j.asr.2005.08.037.
Ma, L., Li, M., Ma, X., Cheng, L., Du, P., Liu, Y., 2017. A review of supervised object-based land-cover image classification. ISPRS J. Photogramm. Remote Sens. 130, 277–293.
Maciel, A.M., Camara, G., Vinhas, L., Picoli, M.C.A., Begotti, R.A., Assis, L.F.F.G.D., 2019. A spatiotemporal calculus for reasoning about land-use trajectories. Int. J. Geogr. Inf. Sci. 33, 176–192.
Mallinis, G., Koutsias, N., Arianoutsou, M., 2014. Monitoring land use/land cover transformations from 1945 to 2007 in two peri-urban mountainous areas of Athens metropolitan area, Greece. Sci. Total Environ. 490, 262–278.
Mendoza, M.E., Granados, E.L., Geneletti, D., Pérez-Salicrup, D.R., Salinas, V., 2011. Analysing land cover and land use change processes at watershed level: a multitemporal study in the Lake Cuitzeo watershed, Mexico (1975–2003). Appl. Geogr. 31, 237–250.
Michishita, R., Jin, Z., Chen, J., Xu, B., 2014. Empirical comparison of noise reduction techniques for NDVI time-series based on a new measure. ISPRS J. Photogramm. Remote Sens. 91, 17–28.
Minnis, P., Doelling, D.R., Nguyen, L., Miller, W.F., Chakrapani, V., 2008. Assessment of the visible channel calibrations of the TRMM VIRS and MODIS on aqua and Terra. J. Atmos. Ocean. Technol. 25, 385–400.
Minnis, P., Trepte, Q.Z., Sun-Mack, S., Chen, Y., Doelling, D.R., Young, D.F., Spangenberg, D.A., Miller, W.F., Wielicki, B.A., Brown, R.R., Gibson, S.C., Geier, E.B., 2008. Cloud detection in non-polar regions for CERES using TRMM VIRS and Terra and Aqua MODIS data. IEEE Trans. Geosci. Remote Sens. 46, 3857–3884.
Mustaphi, C.J.C., Capitani, C., Boles, O., Kariuki, R., Newman, R., Munishi, L., Marchant, R., Lane, P., 2019. Integrating evidence of land use and land cover change for land management policy formulation along the Kenya-Tanzania borderlands. Anthropocene 28, 100228.
Nguyen, L.H., Joshi, D.R., Clay, D.E., Henebry, G.M., 2020. Characterizing land cover/land use from multiple years of landsat and MODIS time series: a novel approach using land surface phenology modeling and random forest classifier. Remote Sens. Environ. 238, 111017.
Novillo, C.J., Arrogante-Funes, P., Romero-Calcerrada, R., 2019. Recent NDVI trends in mainland Spain: land-cover and phytoclimatic-type implications. ISPRS Int. J. Geo Inf. 8, 43.
Ovejero-Campos, A., Fernández, E., Ramos, L., Bento, R., Méndez-Martínez, G., 2019. Methodological limitations of CLC to assess land cover changes in coastal environments. J. Coast. Conserv. 23, 657–673.
Paoletti, M.E., Haut, J.M., Plaza, J., Plaza, A., 2018. A new deep convolutional neural network for fast hyperspectral image classification. ISPRS J. Photogramm. Remote Sens. 145, 120–147.
Pontius Jr., R.G., Shusas, E., McEachern, M., 2004. Detecting important categorical land changes while accounting for persistence. Agric. Ecosyst. Environ. 101, 251–268.
Quintero-Gallego, M.E., Quintero-Angel, M., Vila-Ortega, J.J., 2018. Exploring land use/land cover change and drivers in andean mountains in Colombia: a case in rural Quindío. Sci. Total Environ. 634, 1288–1299.
Ramírez-Cuesta, J.M., Rodríguez-Santalla, I., Gracia, F.J., Sánchez-García, M.J., Barrio-Parra, F., 2016. Application of change detection techniques in geomorphological evolution of coastal areas. example: mouth of the river Ebro (period 1957–2013). Appl. Geogr. 75, 12–27.
Rodrigues, A., Marcal, A.R., Cunha, M., 2016. PhenoSat–a tool for remote sensing based analysis of vegetation dynamics. Multitemporal Remote Sensing. Springer, Cham, pp. 195–215.
Sala, O.E., Chapin, F.S., Armesto, J.J., Berlow, E., Bloomfield, J., Dirzo, R., Huber-Sanwald, E., Huenneke, L.F., Jackson, R.B., Kinzig, A., Leemans, R., Lodge, D.M., Mooney, H.A., Oesterheld, M., Poff, L., Sykes, M.T., Walker, B.H., Walker, M., Wall, D.H., 2000. Global biodiversity scenarios for the year 2100. Science 287, 1770–1774.
Seto, K.C., Satterthwaite, D., 2010. Interactions between urbanization and global environmental change. Curr. Opin. Environ. Sustain. 2, 127–128.
Shao, Y., Lunetta, R.S., Wheeler, B., Iiames, J.S., Campbell, J.B., 2016. An evaluation of time-series smoothing algorithms for land-cover classifications using MODIS-NDVI multi-temporal data. Remote Sens. Environ. 174, 258–265.
Sica, F., Pulella, A., Nannini, M., Pinheiro, M., Rizzoli, P., 2019. Repeat-pass SAR interferometry for land cover classification: a methodology using Sentinel-1 short-time-series. Remote Sens. Environ. 232, 111277.
Teixeira, Z., Teixeira, H., Marques, J.C., 2014. Systematic processes of land use/land cover change to identify relevant driving forces: implications on water quality. Sci. Total Environ. 470, 1320–1335.
Theobald, D.M., Spies, T., Kline, J., Maxwell, B., Hobbs, N.T., Dale, V.H., 2005. Ecological support for rural land-use planning. Ecol. Appl. 15, 1906–1914.
USGS-EROS Center, 2011. MODIS Reprojection Tool User's Manual. Department of Mathematics and Computer Science, South Dakota School of Mines and Technology, Reston, VA.
Vanella, D., Consoli, S., Ramírez-Cuesta, J.M., Tessitori, M., 2020. Suitability of the MODIS-NDVI time-series for an a posteriori evaluation of the citrus tristeza virus epidemic. Remote Sens. 12, 1965.
Venkatappa, M., Sasaki, N., Shrestha, R.P., Tripathi, N.K., Ma, H.O., 2019. Determination of vegetation thresholds for assessing land use and land use changes in Cambodia using the Google earth engine cloud-computing platform. Remote Sens. 11, 1514.
Verbesselt, J., Hyndman, R., Newnham, G., Culvenor, D., 2010. Detecting trend and seasonal changes in satellite image time series. Remote Sens. Environ. 114, 106–115.
Vermote, E., Tanré, D., Deuzé, J.L., Herman, M., Mocrette, J.J., 1997. Second simulation of the satellite signal in the solar Spectrum (6S): an overview. IEEE Trans. Geosci. Remote Sens. 35, 675–686.
Waylen, P., Southworth, J., Gibbes, C., Tsai, H., 2014. Time series analysis of land cover change: developing statistical tools to determine significance of land cover changes in persistence analyses. Remote Sens. 6, 4473–4497.
Wenny, B.N., Sun, J., Xiong, X., Wu, A., Chen, H., Angal, A., Choi, T., Chen, N., Madhaven, S., Geng, X., Kuyper, J., Tan, L., 2010. MODIS calibration algorithm improvements developed for collection 6 level-1B. earth observing systems XI. Proc. SPIE 7807, 78071F-9.
Wolfe, R.E., Roy, D.P., Vermote, E., 1998. MODIS land data storage, gridding, and compositing methodology: level 2 grid. IEEE Trans. Geosci. Remote Sens. 36, 1324–1338.
Xie, Y., Weng, Q., 2016. Updating urban extents with nighttime light imagery by using an object-based thresholding method. Remote Sens. Environ. 187, 1–13.
Xiong, X., Sun, J., Barnes, W., Salomonson, V., Esposito, J., Erives, H., Guether, B., 2007. Multiyear on orbit calibration and performance of Terra MODIS reflective solar bands. IEEE Trans. Geosci. Remote Sens. 45, 879–889.
Xu, Y., Goodacre, R., 2018. On splitting training and validation set: a comparative study of cross-validation, bootstrap and systematic sampling for estimating the generalization performance of supervised learning. J. Anal. Test. 2, 249–262.
Xu, Y., Yu, L., Feng, D., Peng, D., Li, C., Huang, X., Lu, H., Gong, P., 2019. Comparisons of three recent moderate resolution African land cover datasets: CGLS-LC100, ESA-S2-LC20, and FROM-GLC-Africa30. Int. J. Remote Sens. 40, 6185–6202.
Yan, J., Wang, L., Song, W., Chen, Y., Chen, X., Deng, Z., 2019. A time-series classification approach based on change detection for rapid land cover mapping. ISPRS J. Photogramm. Remote Sens. 158, 249–262.
Yang, H., Yang, X., Heskel, M., Sun, S., Tang, J., 2017. Seasonal variations of leaf and canopy properties tracked by ground-based NDVI imagery in a temperate forest. Sci. Rep. 7, 1–10.
Yin, H., Pflugmacher, D., Li, A., Li, Z., Hostert, P., 2018a. Land use and land cover change in Inner Mongolia-understanding the effects of China's re-vegetation programs. Remote Sens. Environ. 204, 918–930.
Yin, H., Prishchepov, A.V., Kuemmerle, T., Bleyhl, B., Buchner, J., Radeloff, V.C., 2018b. Mapping agricultural land abandonment from spatial and temporal segmentation of Landsat time series. Remote Sens. Environ. 210, 12–24.
Zhang, H.K., Roy, D.P., 2017. Using the 500 m MODIS land cover product to derive a consistent continental scale 30 m Landsat land cover classification. Remote Sens. Environ. 197, 15–34.
Zhang, C., Pan, X., Li, H., Gardiner, A., Sargent, I., Hare, J., Atkinson, P.M., 2018. A hybrid MLP-CNN classifier for very fine resolution remotely sensed image classification. ISPRS J. Photogramm. Remote Sens. 140, 133–144.
Zhang, H., Xu, R., 2018. Exploring the optimal integration levels between SAR and optical data for better urban land cover mapping in the Pearl River Delta. Int. J. Appl. Earth Obs. Geoinf. 64, 87–95.
Zhao, W., Du, S., 2016. Learning multiscale and deep representations for classifying remotely sensed imagery. ISPRS J. Photogramm. Remote Sens. 113, 155–165.
Zhou, J., Jia, L., Menenti, M., 2015. Reconstruction of global MODIS NDVI time series: performance of harmonic ANalysis of time series (HANTS). Remote Sens. Environ. 163, 217–228.
Zhu, Z., Woodcock, C.E., 2014. Continuous change detection and classification of land cover using all available Landsat data. Remote Sens. Environ. 144, 152–171. https://doi.org/10.1016/j.rse.2014.01.011.
Zhu, Z., Zhang, J., Yang, Z., Aljaddani, A.H., Cohen, W.B., Qiu, S., Zhou, C., 2019. Continuous monitoring of land disturbance based on Landsat time series. Remote Sens. Environ. 111116.
Zhu, X., Xiao, G., Zhang, D., Guo, L., 2021. Mapping abandoned farmland in China using time series MODIS NDVI. Sci. Total Environ. 755, 142651.